Journal of Macromolecular Science, Part A
Publication details, including instructions for authors and subscription information:
http://www.informaworld.com/smpp/title~content=t713597274

Synthesis and Modeling of Acridine Dyes as Potential Photosensitizers for Dye-Sensitized Photovoltaic Applications

Ravi Mosurkal[a]; Landa Hoke[a]; Stephen A. Fossey[a]; Lynne A. Samuelson[a]; Jayant Kumar[b]; David Waller[c]; Russell A. Gaudiana[c]
[a] U.S. Army Research, Development and Engineering Command, Natick Soldier Center, Natick, MA [b] Center for Advanced Materials, University of Massachusetts Lowell, Lowell, MA [c] Konarka Technologies, Inc., Lowell, MA

To cite this Article Mosurkal, Ravi , Hoke, Landa , Fossey, Stephen A. , Samuelson, Lynne A. , Kumar, Jayant , Waller, David and Gaudiana, Russell A.(2006) 'Synthesis and Modeling of Acridine Dyes as Potential Photosensitizers for Dye-Sensitized Photovoltaic Applications', Journal of Macromolecular Science, Part A, 43: 12, 1907 — 1922
To link to this Article: DOI: 10.1080/10601320600995272
URL: http://dx.doi.org/10.1080/10601320600995272

Journal of Macromolecular Science®, Part A: Pure and Applied Chemistry, 43:1907–1922, 2006

ISSN 1060-1325 print/1520-5738 online
DOI: 10.1080/10601320600995272

Synthesis and Modeling of Acridine Dyes as Potential Photosensitizers for Dye-Sensitized Photovoltaic Applications†

RAVI MOSURKAL,[1] LANDA HOKE,[1] STEPHEN A FOSSEY,[1] LYNNE A. SAMUELSON,[1] JAYANT KUMAR,[2] DAVID WALLER,[3] AND RUSSELL A. GAUDIANA[3]

[1]U.S. Army Research, Development and Engineering Command, Natick Soldier Center, Natick, MA
[2]Center for Advanced Materials, University of Massachusetts Lowell, Lowell, MA
[3]Konarka Technologies, Inc., Lowell, MA

We have synthesized novel aromatic amine-substituted acridine dyes as potential candidates for the photosensitizers in dye sensitized nanocrystalline semiconductor based solar cells (DSSC) cells. The protonation and quaternization of the acridine nitrogen led to acridine dyes with extended absorption from 400–800 nm. Computational modeling was used to evaluate a variety of structures to achieve insights for correlating these types of molecular structures with predicted absorption spectra. Pertinent dihedral angles as well as bond lengths were evaluated to assess and compare planarity and conjugation for these dyes. Other predictions include plots of the HOMO and LUMO levels to qualitatively examine electron distributions and the potential for electron injection. The results from modeling along with the experimental data consisting of synthesis, characterization and UV-visible absorption properties of the selected dyes are presented.

Keywords acridine dyes, dye-sensitized solar cells, modeling, density functional theory

Introduction

Dye sensitized nanocrystalline semiconductor based solar cells (DSSC) developed by Grätzel and coworkers (1) are of immense interest as alternate energy sources. A polypyridyl complex, [$Ru(dcbpy)_2(NCS)_2$, where dcbpy is 4,4′-dicarboxylic bipyridyl], well known as N3 and N719, shows overall photoelectric conversion efficiency of 8–10% when a liquid electrolyte containing I_3^-/I^- solution is used (2–4). Although the ruthenium-bipyridyl type dyes have been some of the most efficient dye sensitizers, it is expensive and the absorption beyond 650 nm is zero. To fully utilize solar radiation, low cost dyes with absorption in longer wavelengths are necessary. Investigations to find non-metalized organic

†Dedicated to the memory of Professor Sukant K. Tripathy.

Address correspondence to Jayant Kumar, Center for Advanced Materials, University of Massachusetts Lowell, Lowell, MA 01854. E-mail: jayant_kumar@uml.edu and Ravi Mosurkal, U.S. Army Research, Development and Engineering Command, Natick Soldier Center, Natick, MA 01760. E-mail: Ravi_Mosurkal@uml.edu

dye sensitizers are of interest to in the fabrication of all organic solid state cells. There has been considerable effort to find organic dyes to use as photosensitizers in DSSC cells (5). Hara et al. (6a) modified a coumarin-343 dye with extended π-conjugation which showed a very high photo-conversion efficiency of 5.6% in a DSSC cell. Recently, they also reported a class of polyene dyes (6b) which showed conversion efficiencies up to 6.8%.

The advantages of pure organic dyes over inorganic/organometallic dyes could be generalized as follows: (i) several commercial dyes are available with a variety of chelating groups for DSSC applications which should lead to a better understanding of structure-property relationships; (ii) most of the organic dyes have very high molar extinction coefficients compared to inorganic complexes, e.g. 10,000–20,000 vs. $>30{,}000\ cm^{-1}M^{-1}$ (iii) modeling using semi-empirical quantum chemical methods as well as *ab initio* and density functional methods for screening and structural modifications is possible; (iv) the absorption energies can be easily modified by varying substituents and conjugation length; (v) better solubility in organic solvents and faster adsorption onto TiO_2; (vi) versatile functionalization onto polymers for preparation of dye-incorporated solid state polyelectrolytes. Although pure organic dyes to date are less efficient than inorganic/organometallic dyes, further development of these types of dyes is critical to the emerging field of DSSC technology.

The synthesis of 9-acridyl derivatives and their anti-tumor activity is known in the literature (7). These acridine derivatives were well studied for their excited state charge transfer properties (8). We have identified a series of acridine dyes (Figure 1) with promising extended absorption for photovoltaic studies. Substitution of a variety of triphenyl amine derivatives at the 9-position on acridine and quaternization of the acridine nitrogen led to dyes with extended absorption and interesting photophysical properties. The following sections will discuss the synthesis, modeling and properties of these new dyes.

Experimental

All the starting materials, catalysts and solvents were purchased from Aldrich and used as received. ^{1}H-NMR spectra were recorded on a Bruker 200 MHz spectrometer. UV-visible spectra were recorded on a Perkin-Elmer (Model Lambda 9) spectrophotometer. FTIR spectra were recorded on a Perkin-Elmer (Model 1720) spectrophotometer.

Synthesis of Dyes 1–5

The synthesis of the dyes, **1**–**3** were carried out following a reported procedure (7). These dyes were characterized by ^{1}H-NMR spectroscopy. The dye **4** was synthesized as follows. In a three-neck round bottom flask, **1** (0.5 g), 4-fluorobenzonitrile (0.46 g) and finely ground cesium fluoride (0.73 g) were dissolved in 10 ml DMSO and under nitrogen atmosphere, the reaction mixture was heated up to 160 C for 2 h. At 50°C, the solution turned dark. After 2 h, the TLC of the reaction mixture showed the appearance of a new compound. The temperature was increased to 185°C and the reaction mixture was heated for a further 2 h. The greenish-brown solution was cooled and poured over ice and stirred for 0.5 h. The resulting greenish solid was filtered, washed several times with water to obtain 0.67 g of dicyano substituted product as shown in Scheme 1. The product was recrystallized from an ethylacetate-hexane mixture. FTIR: 1601 cm^{-1} (C═C stretching), 2225 cm^{-1} (CN stretching); ^{1}H NMR (DMSO-d_6, 200 MHz, ppm), δ 8.26 (d, 2H), 7.80 (m, 8H), 7.61 (m, 4H), 7.45 (d, 2H), 7.43 (d, 2H), 7.32 (d, 2H); UV-Vis ($CHCl_3$ solution): λ_{max} 350 nm.

The dicyano compound (Scheme 1) was hydrolyzed to synthesize dye **4** as follows. The dicyano compound (0.05 g) was placed in a round-bottom flask fitted with a reflux

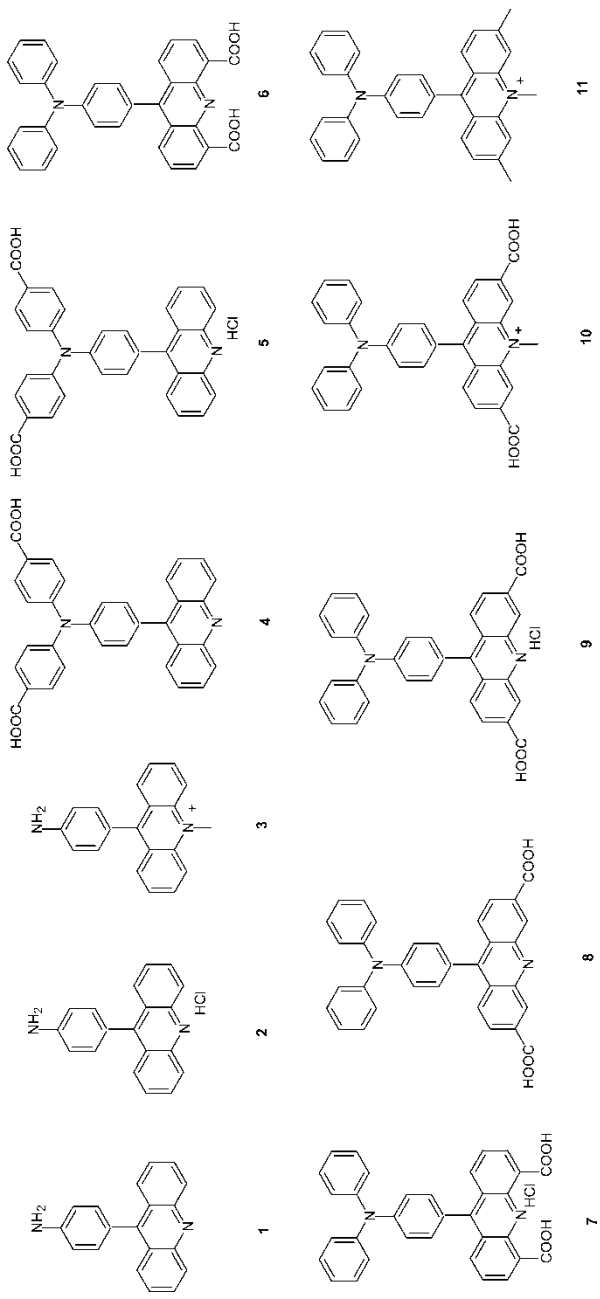

Figure 1. Structures of the acridine dyes of interest.

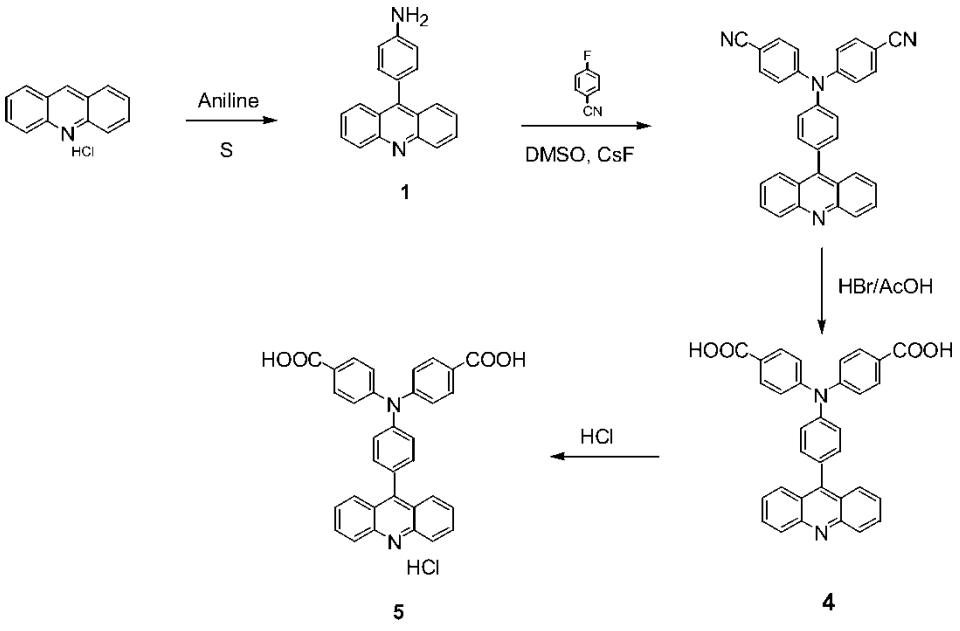

Scheme 1. Synthesis of acridine dyes **1**, **4** and **5**.

condenser, followed by the addition of 1 ml of glacial acetic acid and 1 ml of 48% HBr. The light green slurry was then heated to reflux for 2 h. The TLC clearly indicated the absence of nitrile compound and the appearance of a new spot. The resulting dark green solution was cooled to room temperature and poured into an ice-water mixture, and neutralized with 20% aqueous ammonium hydroxide. The green precipitate obtained was filtered and washed with water. Yield: 0.035 g (70%); FTIR: 1601 cm (C=C stretching), 1657 cm (C=O stretching); ^{1}H-NMR (DMSO-d_6, 200 MHz, ppm): δ 8.25 (d, 2H), 7.92 (m, 6H), 7.83 (d, 2H), 7.64 (d, 2H), 7.48 (m, 2H), 7.39 (m, 2H), 7.26 (d, 2H), 7.20 (d, 2H). UV-vis (ethanol solution): λ_{max} 339 nm ($\varepsilon = 82{,}892\ cm^{-1}M^{-1}$). Protonation of **4** was carried out by exposing to HCl gas until the color of the solution was turned to orange red to indicate the formation of the protonated dye, **5**.

Synthesis of Dyes 8-11

The synthesis of the dye **10** was carried out as shown in Scheme 2. All the intermediate products and the final product were characterized by ^{1}HNMR spectroscopy. A 250 ml round-bottom flask was charged with **a** (10 g, 3.6 mmol), **b** (6.7 g, 44.3 mmol), $Pd_2(dba)_3$ (0.5 g, 0.54 mmol, 3 mol% of Pd), BINAP ligand (0.5 g, 0.81 mmol), cesium carbonate (17.2 g, 53 mmol) in 60 ml of toluene as solvent and heated to 100°C until the disappearance of starting materials (48 h). The reaction mixture was then cooled to room temperature and 180 ml of dichloromethane was added. The mixture was filtered and the filtrate was evaporated to dryness to obtain 13 g. of crude product, **c**. The hydrolysis and cyclization of the above product was carried out in concentrated sulfuric acid and heated to 100°C for 5 h and poured in 300 ml of water to precipitate the product **d**. The product was filtered and washed twice with 300 ml of water and dried under vacuum overnight at 60°C.

N-methylation of **d**: To a stirred solution of **d** (2 g, 7.0 mmol) in 50 ml DMF was added cesium carbonate (9.2 g, 28.4 mmol) followed by iodomethane (14.2 g,

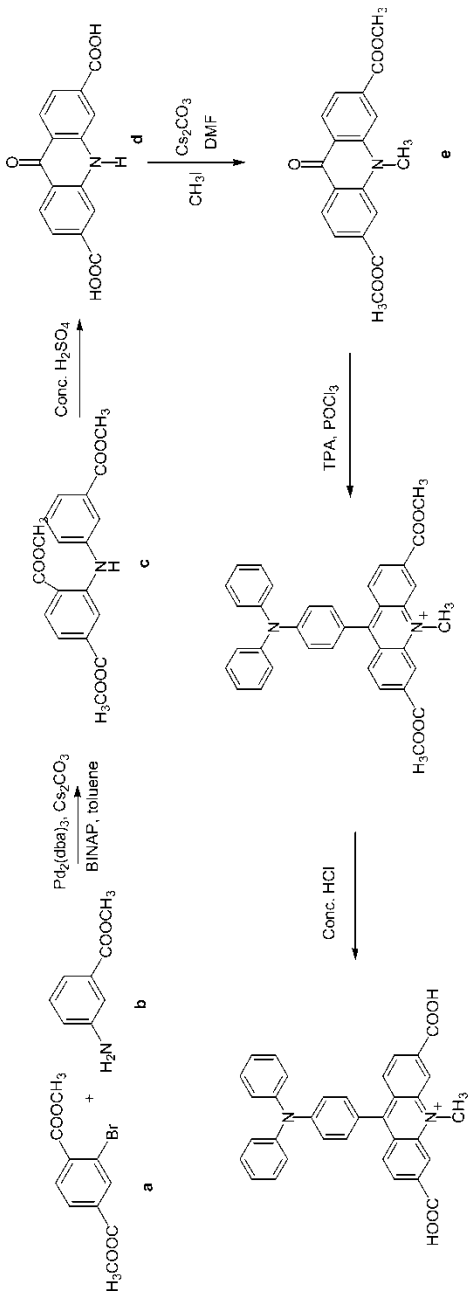

Scheme 2. Synthesis of acridine dye **10**.

100 mmol). The mixture was heated to 40°C for 24 h. It was then cooled to room temperature and 175 ml of ethyl acetate was added and filtered. The precipitate was washed with 100 ml of ethyl acetate and the washings were combined with the filtrate. The combined ethyl acetate solution was washed twice with 250 ml saturated NaCl aqueous solution and dried over anhydrous $MgSO_4$. The solvent was evaporated to give 2.06 g of the product, **e**. This crude product was purified by column chromatography using ethylacetate: hexane (70:30) to give a pure product of **e**.

The coupling reaction of **e** with triphenylamine (TPA) as shown in Scheme 1 was carried out in $POCl_3$ without any solvent. 0.6 g (1.85 mmol) and 0.9 g (3.7 mmol) of triphenylamine were stirred in 30 ml of $POCl_3$ at refluxing temperature for 24 h. The excess $POCl_3$ was evaporated and 50 ml of hexane was added and filtered to separate the insoluble product, **f**. After filtration, the product was dried under vacuum for overnight at 60°C. Purification of the product was carried out on a sephadex column using methanol as solvent. In the final step, the hydrolysis of the ester groups was carried out as follows. 0.1 g of **f** was dissolved in 7 ml of methanol, 14 ml of distilled water and 2.5 ml of concentrated HCl and the mixture was heated to 60°C under nitrogen atmosphere for 17 h and the solvents were evaporated under vacuum to give the desired dye, **10**. ^{1}H-NMR (DMSO-d_6, 200 MHz, ppm): δ 9.2 (s, 2H), 8.9 (d, 2H), 9.2 (s, 2H), 8.4 (m, 4H), 8.1 (d, 2H), 7.5 (d, 4H), 7.3 (m, 2H), 7.1 (d, 4H), 4.9 (s, 3H); UV-Vis (Methanol solution): λ_{max} 617 nm ($\varepsilon = 4{,}522\ cm^{-1}M^{-1}$). The synthesis of dye **11** was carried out using the above procedure and the appropriate starting materials.

Modeling

Methods. Modeling studies were undertaken concurrently with dye synthesis. Calculations were conducted in an attempt to understand the effects of chemical structure on the longest wavelength absorption and provide insight into the performance of the dyes as sensitizers in DSSC. Calculations were carried out on a series of dye molecules and also precursor molecules (Figure 1).

Geometry Optimization. All calculations were performed using the Gaussian 03 code. Geometries were optimized using density functional theory (DFT) using the B3LYP functional and the 6-31g* basis set (B3LYP/6-31G*). The longest wavelength absorption was expected to correlate with a more planar structure. In particular, the dihedral angle between the acridine moiety and the attached phenyl ring will be related to extended conjugation (see Figure 6).

UV-Visible Absorption Spectra Prediction. Gas phase UV-vis absorption spectra were calculated using three methods: the semi-empirical method Zerner's Intermediate Neglect of Differential Overlap/Spectra (INDO/S), *ab initio* Configuration Interaction Singles (CIS), and Time Dependent Density Functional Theory TD-DFT. Solvent effects were accounted for using the Self-Consistent Reaction Field (SCRF) Polarized Continuum Model (PCM).

Results and Discussion

Synthesis

The simple synthesis of 9-(4-aminophenyl)-acridines was carried out by heating a 10-protonated acridine with sulfur at 120°C and gave good yields (~80%) of **1**.

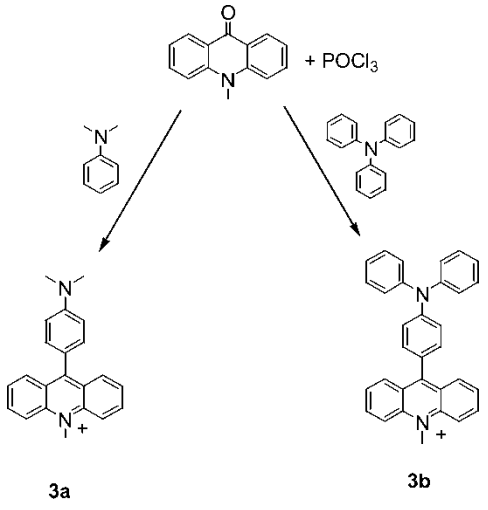

Scheme 3. Coupling of N-methylacridone with *p*-tertiary amine substituted phenyl groups.

The subsequent step of cyano functionalization was achieved by the reaction of **1** with 4-cyanofluorobenzene in the presence of cesium fluoride in good yield (~70%). The resulting cyano substituted dye was hydrolyzed to COOH groups using a HBr/glacial acetic acid mixture to obtain the desired final product, **4**. To further improve the absorption, the dye **4** was protonated on the acridine nitrogen by exposure to HCl gas.

The synthesis of acridine dyes with COOH groups on the acridine moiety was achieved by the 5 step synthesis shown in Scheme 2. The substitution of COOH groups on the acridine side of the molecule is advantageous due to the electron accepting nature of the acridine ring. This will be discussed in detail in the following sections. The first step of the synthesis was carried out following the Buchwald reaction using Pd as catalyst in the presence of a base and BINAP ligand. Cyclization was followed by N-methylation to result in *N*-methylacridone. The coupling of triphenylamine was achieved with *N*-methyl acridone in a simple and single step synthesis phosphorous oxychloride and no solvent.

It is believed that in this reaction, the 9-chloroacridine dichlorophosphonic acid salts are formed as intermediates that readily react with amine containing aromatic compounds immediately (9). This reaction was first tested on a simple commercially available *N*-methylacridone to prepare the dyes **3a** and **3b** as shown in Scheme 3. 3,6-Dimethyl-*N*-methylacridone, synthesized according to Scheme 2 was used to prepare the dye, **11**, using the above scheme.

UV-Visible Absorption Studies

The UV-visible absorption spectra of precursor molecules **1**–**3** were measured in ethanol solution and are shown in Figure 2a. As can be seen from the spectra, the λ_{max} values are shifted to longer wavelength as the precursor dye, **1** was protonated in **2** and quaternized in **3**. This shift in wavelength is attributed to the resonance of charge transfer from acridine nitrogen to the amino nitrogen as shown in Figure 3. The charge transfer phenomenon was suggested in these types of protonated and quaternized acridine dyes previously by Acheson et al. (10).

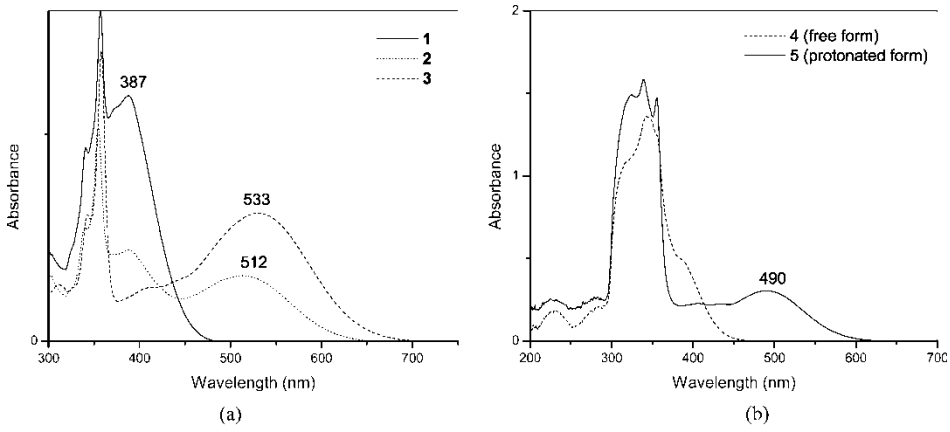

Figure 2. UV-visible absorption spectra of (a) **1**, **2** and **3** (b) **4** and **5** in ethanol solution.

In Figure 4a, UV-visible spectra of the dyes, **3**, **3a** and **3b** measured in ethanol solution were compared. Here the substitution of nitrogen on the donor amino group of these dyes is changed from NH_2 to dimethylamino and finally to diphenylamino. It is interesting to note that as the donor strength of the amino group is changed from primary (**3**) to the tertiary amine (**3a**), the absorption is red shifted about 34 nm. However, the substitution of phenyl groups on **3** only red shifted 16 nm due to the weak mesomeric effect of phenyl groups in **3b** compared to methyl groups in **3a**.

Figure 4b shows the absorption spectra of the dyes **9** and **10** in methanol. It is quite interesting to see the tremendous shift in absorption (~60 nm) in these final quaternized dyes compared to **3b**. The substitution of acceptor groups such as COOH on the acridine moiety at the 3,6 positions further shifts the absorption in these dyes and makes them potential candidates for harvesting light in the entire visible and near IR region for photovoltaic applications. A model dye, **11** was synthesized which is substituted with methyl groups at the 3 and 6 positions on the acridine moiety. Although this dye has a promising absorption spectrum (Figure 5) it cannot be used for PV applications due to the absence of chelating groups.

Modeling

Precursors. Figure 1 shows the structures of all the molecules evaluated with modeling. Molecules **1**, **2**, and **3** are referred to as precursors and molecules **4** through **10** were

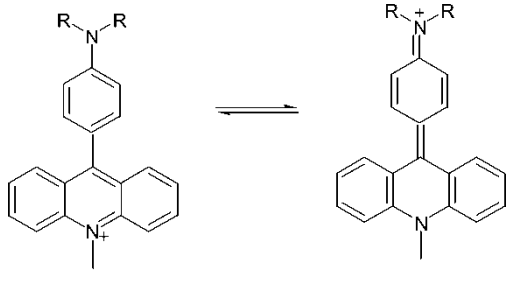

Figure 3. Delocalization of charge in protonated/quaternized acridine dyes.

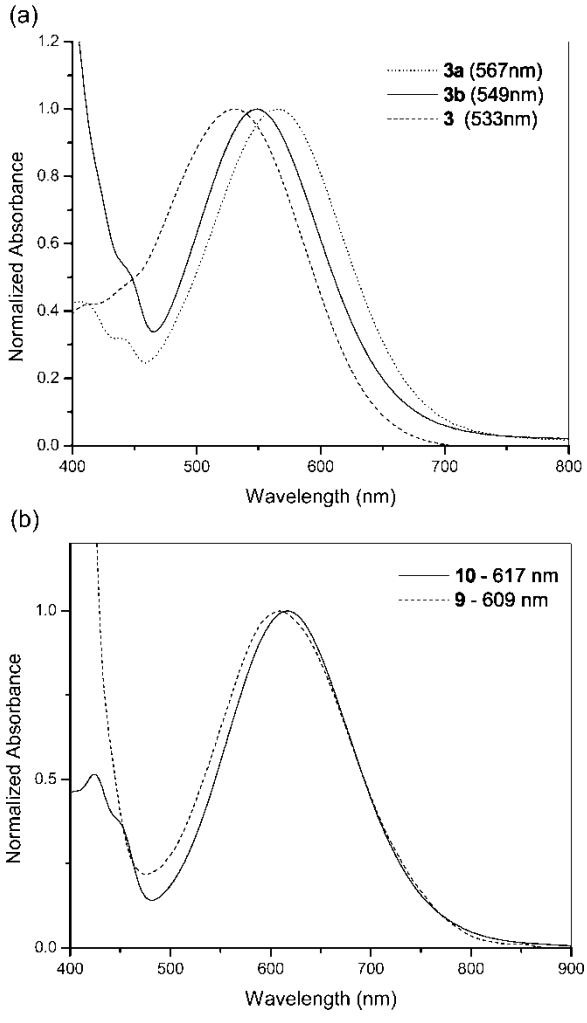

Figure 4. UV-visible absorption spectra of (a) **3**, **3a** and **3b** in ethanol (b) **9**, **10** in methanol solution.

considered dye candidates. The calculated dihedral angle and bond length for the bond connecting the acridine moiety and the phenyl ring for the precursors are shown in Table 1 (see Figure 6 for the location of the bond). Geometry changes associated in protonating **1** to obtain **2** include a decrease in the dihedral angle from 66 degrees to 52 degrees. This decrease in dihedral angle suggests that **2** become more conjugated and therefore a longer absorption wavelength might be expected. Methylating **2** gives **3**. The dihedral angle for **3** is 54 degrees slightly less planar than **2**.

Predicted longest wavelength UV-vis absorbance is shown in Table 2. Experimentally and for each of the three methods of calculating the UV-Vis absorbance spectra, protonation causes a red shift. That result is in contrast to a recent study of 9-aminoacridine and acridine-9-*N*-methacrylamide dyes where only a slight blue shift was seen upon protonation (11). Experimental data show that the longest wavelength absorption for **3** is somewhat longer than that of **2**. The increase cannot be explained based on a decrease in the magnitude of the dihedral angle between the acridine and phenyl groups (i.e., increased

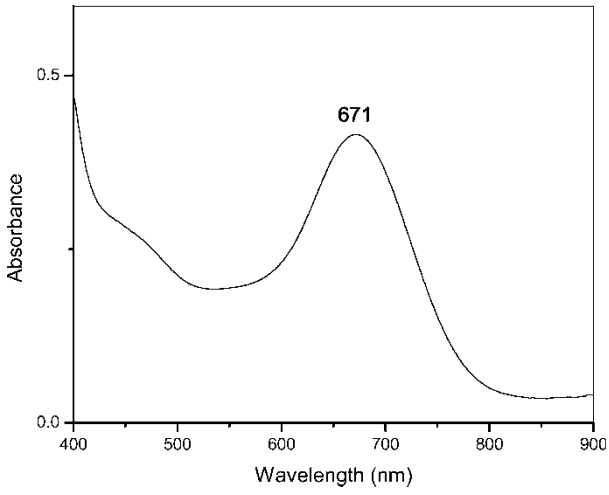

Figure 5. UV-visible absorption spectra of **11** in ethanol solution.

conjugation). Adding the methyl group lowers the gap between the HOMO and the LUMO for **3** compared to **2** and is reflected in the increase in wavelength. TD-DFT calculations, shown in Table 2, predict longer wavelength absorption for **3** as compared to **2**.

For **1**, TD-DFT calculations suggest that the main contribution to the lowest energy absorption is the HOMO to the LUMO, but there is also a smaller contribution from the HOMO-1 to the LUMO. Protonating and methylating this structure produces positively charged molecules (**2** and **3**). The lowest energy absorption wavelength is increased in going from **1** to **2** and then again by a smaller amount in going from **2** to **3**. TD-DFT theory predicts that there is only one significant contribution to the lowest energy absorption for **2** and **3** and that is from the HOMO to the LUMO. The other configuration the HOMO-1 to the LUMO that was evident for **1** is no longer contributing to the absorption for **2** and **3**.

In addition to the gas phase, absorptions were calculated in the solvent ethanol because our experimental spectra were measured in this solvent. Compared to modeling predictions in the gas phase, adding the solvent effect increases (at least by a small amount) the absorption wavelength. The trend found for the gas phase that the longest wavelength absorption increases upon protonation (molecule **2**) and further increases after methylation (molecule **3**) is predicted for all cases using the TD-DFT method; although, the semi-empirical and *ab initio* methods do not predict this increase upon methylation. The predictions for ethanol for the CIS method provide results that have significantly shorter wavelengths than observed experimentally. The predictions for

Table 1
Geometry of precursors (see Figure 6 for bond location)

Molecule	**1**	**2**	**3**
Bond length	1.49 Å	1.46 Å	1.47 Å
Dihedral	66°	52°	54°

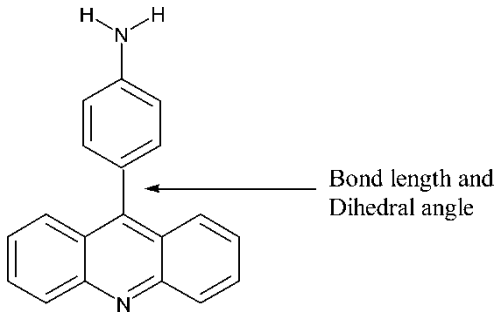

Figure 6. Selected bond and dihedral angle for precursors.

ethanol as compared to experimental results using the TD-DFT method provide a closer correspondence to the observed results and are approximately 45 nm longer than the experimental data for each case, but the correct trend is predicted. Although the semi-empirical results are not as good as the TD-DFT calculations for these molecules, the computational cost of semi-empirical calculations is much lower.

A recent study has been published that includes results for **3** (12). A comparison of our results with these reported results shows agreement with predictions for **3**. Our optimized B3LYP/6-31G* geometry for this structure is in agreement with a value of 54 degrees. In addition, our semi-empirical lowest energy absorption using G03 ZINDO is 2.57 eV compared to their reported value of 2.62 eV obtained using INDO/S in G98. Further, our *ab initio* CIS value for this absorption is 3.75 eV, which is identical to the value reported in this paper.

Acridine Dyes. In this section we present the modeling results for the acridine dyes. The bond lengths and dihedral angles for selected bonds are presented in Table 3. The location of the bonds is shown in Figure 7. The behavior with regard to protonation and methylation is similar to that found for the precursors. Shorter bond lengths and more planar torsion angles are in general associated with longer wavelength absorptions and these geometric effects account for the effects of protonation but not methylation on the lowest energy absorption. The results suggest that based on these geometric

Table 2
Predicted and experimental longest wavelength absorptions.
Oscillator strengths are shown in parentheses

Molecule	ZINDO (gas)	CIS (gas) HF/6-31 g*	CIS (EtOH) hf/6-31 g*	TDDFT (gas) b3LYP/6-31 g*	TDDFT (EtOH) b3lyp/6-31 g*	Exp (EtOH)
1	374 nm	291 nm	296 nm	397 nm	434 nm	387 nm
	(0.35)	(0.31)	(0.39)	(0.14)	(0.13)	
2	482	331	330	554	558	512
	(0.44)	(0.59)	(0.68)	(0.26)	(0.32)	
3	482	331	332	568	578	533
	(0.42)	(0.59)	(0.68)	(0.25)	(0.30)	

Table 3
Comparison of bond lengths (Å) and angles (degrees) for acridine dyes

Molecule	**4**	**5**	**6**	**7**	**8**	**9**	**10**	**11**
Bond length #1	1.49	1.46	1.49	1.46	1.49	1.46	1.46	1.47
Dihedral #1	68	52	65	51	65	49	50	52
Bond length #2	1.43	1.39	1.41	1.38	1.41	1.38	1.38	1.39
Dihedral #2	46	24	35	20	36	20	21	22

considerations, **9** will have a longer wavelength absorption than **5** and this is borne out by the experimental results.

The calculated and measured longest wavelength absorptions are presented in Table 4. Note that not all compounds were synthesized. The semi-empirical gas phase calculations provide the observed trends for comparing protonated and unprotonated molecules. CIS is also able to effectively predict these trends for the longest wavelength absorptions, but all these values are strongly blue shifted relative to the experimental values. TD-DFT results predict trends correctly, except for the absorption wavelength trend for structure **11**, but are red shifted relative to the experimental results. In addition, as we found for the precursors, whereas the semi-empirical and *ab initio* methods fail to account for the observed wavelength increase upon methylation of the acridine nitrogen, TD-DFT does account for this. Because our experimental results were collected in the two solvents ethanol and methanol, we predicted absorptions using the TD-DFT method for both of these solvents. The predictions for these two solvents were very similar, as expected. In the case of these dye molecules inclusion of solvent effects significantly improves agreement with experimental results.

Even though the absolute values of the predicted maximum wavelength absorptions are too large, TD-DFT provides relative longest wavelength absorptions that follow the experimental trends with one exception and so provide a basis for guidance for synthetic efforts.

Some specific comparisons between the modeling and experimental results are as follows. Protonation of **4** to give **5** is predicted to increase the absorption wavelength experimentally and for all modeling methods. Methylation of **9** to give **10** results in a small increase in wavelength that is predicted by the TD-DFT method.

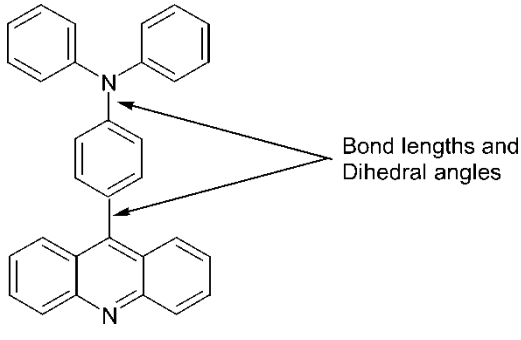

Figure 7. Selected bond lengths and dihedral angles for acridine dyes.

Table 4
Calculated and measured absorptions for acridine dyes. Oscillator strengths are shown in parentheses

Molecule	ZINDO (gas)	CIS (gas) hf/ 6-31 g*	CIS (EtOH) HF/6-31 g*	TDDFT (gas) b3LYP/6-31 g*	TDDFT (EtOH) b3lyp/ 6-31 g*	TDDFT (MeOH) b3lyp/6-31 g*	Exp (EtOH)
4	374 nm (0.45)	292 nm (0.40)	296 nm (0.47)	408 nm (0.18)	433 nm (0.16)	433 nm (0.15)	339 nm
5	523 (0.52)	343 (0.85)	326 (0.89)	724 (0.39)	603 (0.44)	599 (0.44)	460
6	389 (0.57)	297 (0.56)	300 (0.66)	499 (0.12)	555 (0.13)	556 (0.13)	—
7	567 (0.53)	361 (0.84)	342 (0.96)	759 (0.41)	702 (0.46)	698 (0.45)	—
8	392 (0.41)	303 (0.32)	310 (0.39)	533 (0.09)	597 (0.10)	597 (0.10)	
9	600 (0.61)	393 (0.60)	371 (0.95)	764 (0.48)	727 (0.51)	723 (0.50)	609[a]
10	601 (0.57)	393 ((0.88)	346 (0.85)	787 (0.47)	762 (0.51)	757 (0.50)	617[a]
11	532 (0.511)	346 (0.85)	332 (0.94)	708 (0.41)	645 (0.45)	640 (0.45)	671

[a]Measured in methanol.

Including solvent in the calculation brings the wavelengths closer to the observed values. Neither ZINDO nor CIS (gas) were able to predict this increase, and, furthermore, including solvent in this CIS calculation actually resulted in the prediction of a small decrease in wavelength. Evidently, the HF/B3LYP CIS SCRF PCM method is not sufficient to predict absorption for this case.

With regard to comparing the absorption wavelength for **10** and **11**, experimental data suggest an approximately 70 nm increase. All three computational methods in all media (gas or solvent) predict a decrease in wavelength for this case. Therefore, for this case, the trend predicted by modeling is not in agreement with experimental data. Calculations for the analogous structures for the precursors predicted similar trends as we report here for the actual dye molecules (these calculations are not included here). Possibly contributions to the absorption from different resonance structures might be a contributing factor to the different trends predicted by modeling and experiment for this case.

The configurations that make significant contributions to the lowest energy absorption are in all cases, except **4,** the HOMO to the LUMO. For **4** in the gas phase there is also a smaller contribution of the HOMO-1 to LUMO.

Table 5 compares results for HOMO and LUMO energies for protonated and methylated structures (**9** and **10**). These values are based on the optimized ground structure and the associated occupied and virtual orbitals. Because the primary contributing configuration to the lowest energy absorption is the HOMO to the LUMO, these energies can provide qualitative information about this absorption before methods such as TD-DFT are implemented. As we noted for the precursors, methylation reduces the energy gap between the HOMO and the LUMO. Table 5 also shows that this same effect is present for the acridine dye **9** and **10**. Table 5 shows that solvation in ethanol significantly raises the energies of the HOMO and the LUMO but still retains the characteristic that methylation reduces the energy gap between the HOMO and the LUMO.

Insights for dye behavior can be achieved using molecular orbital pictures. Even though, strictly speaking, the molecular orbitals calculated are only mathematical constructs without physical reality they provide qualitatively useful information for rationalizing the properties of molecules (13). Figure 8 shows plots of the HOMO and LUMO for **5** and **9**. For **9** the HOMO is located mostly on the triphenyl amine moiety of the dye, while the LUMO is located on the acridine portion of the dye. For **5** they are reversed. As mentioned previously the COOH groups are used to attach the dye molecules to the semiconductor surface. It is beneficial for electron transfer to have the LUMO near the semiconductor surface. The **9** dye is predicted to be superior to the **5** dye for electron injection because the LUMO is near the COOH binding groups, while the converse is true for **5**.

Table 5
Comparison of HOMO and LUMO levels for protonated and methylated structures

Molecule	**9**	**10**
HOMO (gas)	−7.901 eV	−7.837 eV
LUMO (gas)	−6.187	−6.157
HOMO (EtOH)	−5.517	−5.538
LUMO (EtOH)	−3.567	−3.672

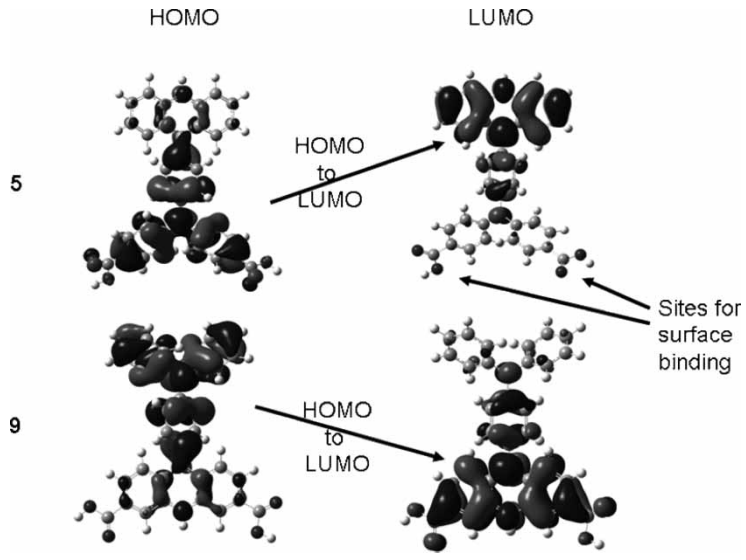

Figure 8. Frontier orbital isosurface plots for protonated molecules **5** and **9**.

Conclusions

We have synthesized and characterized novel acridine dyes and conducted modeling calculations. These dyes show promise as organic photosensitizers. We explored a simple aryl-aryl coupling method to prepare various quaternized acridine dyes using N-methylacridones. The protonation and quaternization of some of these acridine dyes extended the UV-visible absorption spectra further into visible and near-IR region. We have used three methods for modeling to predict geometries and absorptions. The semi-empirical and *ab initio* methods predicted correct trends except for the observed increase in wavelength upon methylation and for the experimental trend for structure **11**. The TD-DFT method was able to account for this increase in wavelength upon methylation, but not the trend observed for structure **11**. We are currently studying these interesting dyes further for their photovoltaic and other opto-electronic applications.

In addition to the photovoltaic and opto-electronic applications investigated here, the absorption change of these dyes upon protonation, demonstrated in this current work, suggests that these dyes also have potential application as chemical sensors.

Acknowledgements

We acknowledge the assistance of the ARL and ASC HPC for computing hours required for this work. Dr. Mosurkal also thanks DARPA for financial support and the National Research Council and the U.S. Army Natick Soldier Center RDECOM for a Senior Research Associateship Award.

References

1. Hagfeldt, A. and Grätzel, M. (1995) *Chem. Rev.*, 95: 49.
2. Hagfeldt, A. and Grätzel, M. (2000) *Acc. Chem. Res.*, 33: 269.

3. Nazeerudin, M.K., Kay, A., Rodicio, I., Humphry, B.R., Mueller, E., Liska, P., Vlachopoulos, N., and Gratzel, M. (1993) *J. Am. Chem. Soc.*, 115: 6382.
4. Mosurkal, R. (2001) *Resonance*, 76.
5. (a) Ferrere, S., Zaban, A., and Gregg, B.A (1997) *J. Phys. Chem.*, 101: 4460; (b) Cherepy, N.J., Stemstad, G.P., Gratzel, M., and Zhang, J.Z. (1997) *J. Phys. Chem. B*, 101: 9342; (c) Sayama, K., Hara, N., Mori, M., Satsuki, S., Suga, S., Tsukagoshi, S., Abe, Y., Sugihara, H., and Arakawa, H. (2000) *Chem. Commun.*, and 1173; (d) Mosurkal, R., Kumar, J., and Samuelson, L. (2004) *J. Photochem. Photobiol. Chemistry.*, 168: 191.
6. (a) Hara, K., Sayama, K., Ohga, Y., Shinpo, A., Suga, S. and Arakawa, H. (2001) *Chem. Commun.*, 569; (b) Hara, K., Kurashige, M., Ito, S., Shinpo, A., Uga, S., Sayama, K., and Arakawa, H. (2003) *Chem. Commun.*, 252.
7. Acheson, R.M. and Birtwistle, D.H. (1986) *J. Chem. Res.*, 3425.
8. Herbich, J. and Kapturkiewicz, A. (1998) *J. Am. Chem. Soc.*, 120: 1014.
9. Gleu, K. and Schubert, A. (1940) *Ber.*, 73B: 757.
10. Acheson, R.M. and Robinson, M.J.T. (1956) *J. Chem. Soc.*, 484.
11. Oliveira, H.P.M. and Camargo, A.J. (2004) *de J. Mol. Struct. (Theochem)*, 674: 213.
12. Lappe, J., Cave, R.J., Newton, M.D., and Rostov, I.V. (2005) *J. Phys. Chem. B*, 109: 6610.
13. Foresman, J.B. and Frisch, A. (2006) *Exploring Chemistry with Electronic Structure Methods*; Gaussian Inc.: Pittsburgh, PA, 19.